In Situ X-Ray Emission Spectroscopy of Battery Materials

Colleen Werkheiser
Department of Physics, University of Washington

(Dated: August 27, 2015)

X-ray emission spectroscopy measurements were taken of $LiMn_2O_4$ and a pouch cell battery ($Li_{1-x}Co_{1/3}Ni_{1/3}Mn_{1/3}O_2$) *in situ* using a tabletop apparatus. The apparatus is a laboratory-based Rowland-circle monochromator with a low power x-ray (bremsstrahlung) tube source, a spherically bent crystal analyzer, and a solid-state detector. The K-$\beta_{1,3}$ and K-β' peaks for both materials, as well as some of the valence features, are resolved in the spectra. This was the first *in situ* measurement of a pouch cell battery and showed that these measurements may be taken using this tabletop system.

I. INTRODUCTION

X-ray emission spectroscopy (XES) has been used to study transition metal complexes, which are materials that are currently being used for battery research. This technique is useful because the spectra obtained are element specific and sensitive to the metal oxidation and spin state, as well as the local geometry of the material [1]. These measurements are typically made at synchrotron x-ray light sources with high brilliance and fine time resolution. However, this study used a new tabletop apparatus that was previously shown to obtain results at synchrotron-level quality, though the data is taken at a much slower rate [2].

The battery materials studied were those used in lithium ion batteries. There is a growing market for these materials because there is a demand for cheaper, more sustainable battery materials. Lithium ion batteries are currently being used in the portable electronics market and may be broadened to be used in electric and hybrid electric vehicles [3]. However, before this can occur there must be improvements made to their energy density, power capability, calendar-life performance, safety, and cost [4]. In order to develop these new materials, there must be an understanding of their electronic structure, which is what XES provides.

The pouch cell battery used in this study is currently being used in the portable electronics market. This battery consists of conductive foils welded to the electrode that carry the positive and negative terminals to the outside of the battery. The active materials are thin foils rather than liquids, and the whole pouch is vacuum sealed. This design has the highest packaging efficiency among battery packs and is very light, but is limited in that it is sensitive to high heat and humidity.

The goal of this study was to measure one lithium ion battery material and to take the first XES measurement of a pouch cell battery. The battery material used was $LiMn_2O_4$ in different charge states in order to determine how this material was affected by different charging curves. The pouch cell battery contained $Li_{1-x}Co_{1/3}Ni_{1/3}Mn_{1/3}O_2$, and the measurements taken focused on the cobalt specifically. Spectra of both of these materials were taken, and the K-$\beta_{1,3}$ and K-$\beta_{2,5}$ peaks were observed.

II. THEORY

X-ray emission spectroscopy is the process in which an incoming x-ray is absorbed and excites an inner-shell electron into an empty electronic state. The electron hole that was created from this process is then filled by an electron from a higher orbital, such as a 2p electron filling the 1s hole. This process is illustrated in Fig . 1. This causes a fluorescence that is detected. Therefore, the spectrum obtained gives information about the density of occupied electronic states in the material. In this process, the known quantities are the energy of the incident photon, Ω, and the energy of the emitted photon, ω. Therefore, $\Omega - \omega$ is the energy that remains in the sample after the x-ray emission process. Then, theoretical considerations assign electron configurations to these energy levels.

One type of fluorescence is the K fluorescence in which an electron is removed from the K shell (1s orbital). The emission lines are then further differentiated by their intensities and given names α, β, γ, etc. with α being the most intense. The lines measured in this study were K-β lines that show strong interactions between the 3p and 3d orbitals that separate the K-$\beta_{1,3}$ and K-β' features. The K-$\beta_{1,3}$ peak gives information about the oxidation state and the K-β' about the local 3d spin. These lines also show weak features at higher energies from transitions between the valence orbitals and the 1s shell, which are denoted as K-$\beta_{2,5}$ and K-β" [5]. These are sensitive to electronic structure and local coordination. The K-β" specifically gives information about the ligand type and distance.

The K-$\beta_{1,3}$/K-β' and K-$\beta_{2,5}$/K-β" features were observed for both $LiMn_2O_4$ and the pouch cell battery (containing $Li_{1-x}Co_{1/3}Ni_{1/3}Mn_{1/3}O_2$) and this data is discussed.

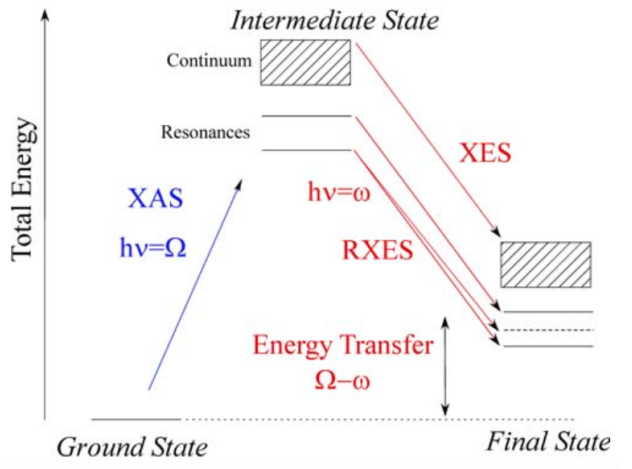

FIG. 1. Basic energy scheme for absorption of a photon of energy Ω and emission of photon with energy ω. The total energy of the system is given on the vertical axis. The dashed line denotes an interaction between valence electrons and the core hole. The portion of this schematic relevant to this study is that labeled XES. Figure taken from "X-ray emission spectroscopy" by Bergmann and Glatzel [5].

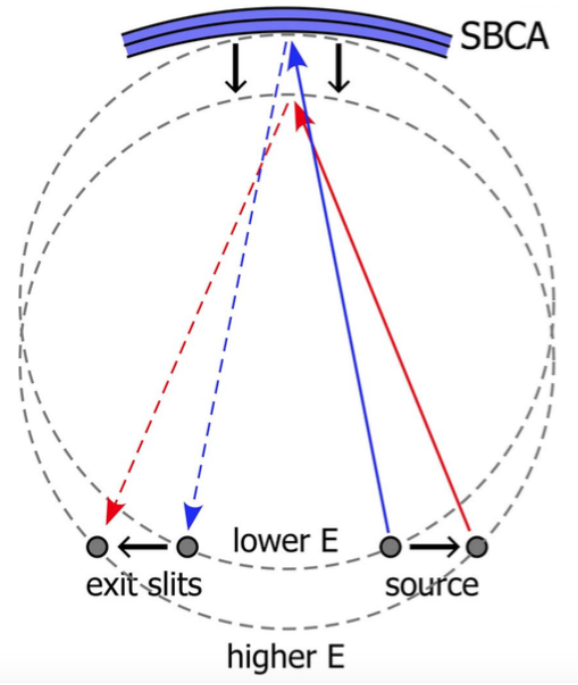

FIG. 2. Energy scanning of the Rowland circle monochromator by synchronized linear motion of the source (and sample), the exit slits (and detector), and the SBCA. Figure taken from "A laboratory-based hard x-ray monochromator for high-resolution x-ray emission spectroscopy and x-ray absorption near edge structure measurements" by Seidler et. al. [2].

III. METHODS

A. Apparatus

The apparatus used was a Rowland-circle monochromator, as shown in Fig. 2 with a low power x-ray tube source, a spherically bent crystal analyzer (SBCA) and solid-state detector. In order to energy scan, the source and detector are moved symmetrically while small adjustments are made to the SBCA such that the Rowland circle geometry is constantly maintained.

A schematic of the XES configuration is given in Fig. 3. The sample is on a manual stage that allows for better alignment. The SBCA is mounted on a two-axis tilt stage that also aids in alignment. The source/sample, SBCA, and detector are each mounted on positioners that maintain the Rowland circle geometry. The x-ray source is a small, air-cooled tube source with an Au anode. The source spot is approximately 0.4 mm × 0.4 mm with a maximum accelerating potential and electron current of 50 kV and 0.2 mA, respectively, for a peak power of 0.01 kW. The SBCA used was particular to each sample being studied, but all had a 1 m radius of curvature, which was also the distance from the source and detector to the analyzer. The detector used was a silicon drift detector with a 25 mm^2 active area and with integrated signal processing electronics. It s important to note that most of the flight path of the x-rays is through helium rather than air, which is significantly less absorbing of x-rays. There is a welded helium box that encompasses 80% of the total linear travel that is not shown in the schematics. The entire apparatus is contained in a radiation enclosure that is fabricated from lead-lined plywood. It includes safety interlock switches that are connected to the x-ray source controller. The entire enclosure is 170 cm long, 81 cm wide, and 61 cm tall. In order to reduce background noise, there is also additional shielding around the source and sample. This shielding is a 3D printed, plastic enclosure covered in lead tape. The exact size and shape of the shielding is dependent upon the sample being studied, with a larger and more complicated setup for the pouch cell battery due to the fact that the active part of the battery is small compared to its overall size.

B. Pouch Cell Battery

The pouch cell battery used was produced at Argonne National Labs and a diagram of it is shown in Fig. 4. The pouch itself is aluminum coated in a polymer. The active cathode is $Li_{1-x}Co_{1/3}Ni_{1/3}Mn_{1/3}O_2$ on an aluminum foil. The anode is graphite on a copper foil. These active layers are separated by a thin plastic insulator. The whole battery is 7 cm × 9 cm. The active layers take up less than a third of the total area of the pouch cell, as shown in Fig. 5.

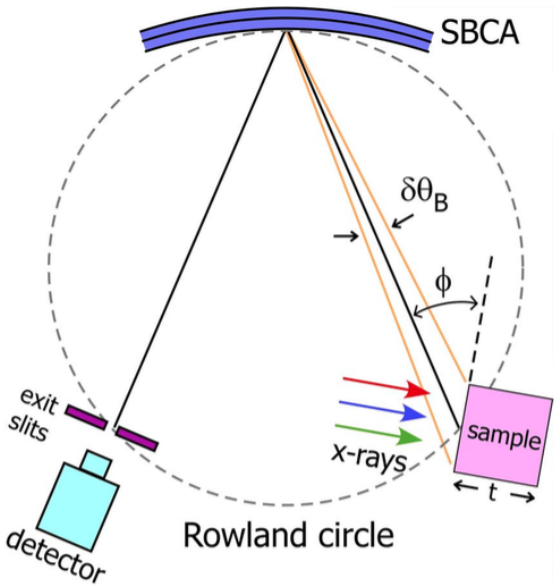

FIG. 3. Experimental setup for x-ray emission spectroscopy. The x-ray source is incident on the face of an idealized sample of thickness t. The resulting emission is analyzed by the spherically bent crystal analyzer (SBCA) and refocused onto the detector. Energy scanning is implemented as described in Fig. 2. Figure taken from "A laboratory-based hard x-ray monochromator for high-resolution x-ray emission spectroscopy and x-ray absorption near edge structure measurements" by Seidler et. al. [2].

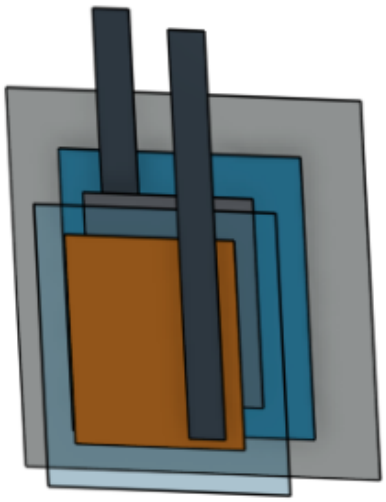

FIG. 4. Rendering of the inner layers of the pouch cell battery. The light gray is the outer aluminum layer. The blue material is the plastic insulators. The darker gray is the aluminum active cathode layer (with the lithium material), and the orange is the copper and graphite anode layer. The dark gray tabs are the current collectors that extend out of the pouch cell to be connected into the circuit. The active layers are not to scale in reference to the outer aluminum.

FIG. 5. Photograph of the pouch cell battery. The raised material in the center is where the active layers are located. The collector currents extend to the outside of the pouch cell.

IV. RESULTS AND DISCUSSION

A. $LiMn_2O_4$

Spectra were taken of $LiMn_2O_4$ in three different charge states over the K-$\beta_{1,3}$ and valence regions. The first sample was a pristine sample, meaning it was fully discharged and had not yet been charged at all. The second had been charged at a rate of C/25 and the third at a rate of C/50. This means that at this rate it would take 25 and 50 hours, respectively, for the sample to be fully charged. A plot of the K-$\beta_{1,3}$ and K-β' features for these samples are shown in Fig. 5. The K-β' feature suggests that the pristine sample is in the highest spin state, then the C/25 sample, then the C/50 with the lowest 3d spin. This is consistent with a pristine versus charged sample. However, the exact charge state of the C/25 and C/50 samples were unknown, but the C/50 was more charged than the C/25, just at a slower rate. Therefore, the trends seen in the spectrum are consistent with the expectations. Fig. 6 shows a close-up of the K-$\beta_{1,3}$ feature. The C/25 and C/50 peaks are shifted to the left, indicating a higher oxidation state, as expected. The C/50 sample is in the highest oxidation state because it was charged more than the C/25 sample. More qualitative analysis will need to be done in order to determine the specific oxidation state of each sample, but more reference samples are needed in order to do so.

The valence features were also observed and are shown in Fig. 7, with the higher peak being the K-$\beta_{2,5}$ and the smaller being the K-β". These show clear differences between the two samples, but further analysis must be done in order to determine the nature of those differences.

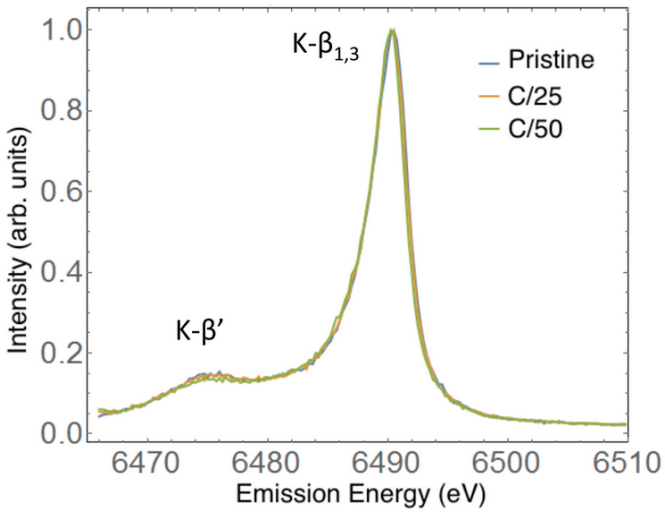

FIG. 6. Plot of the K-$\beta_{1,3}$ and K-β' features for $LiMn_2O_4$ at three different charge states.

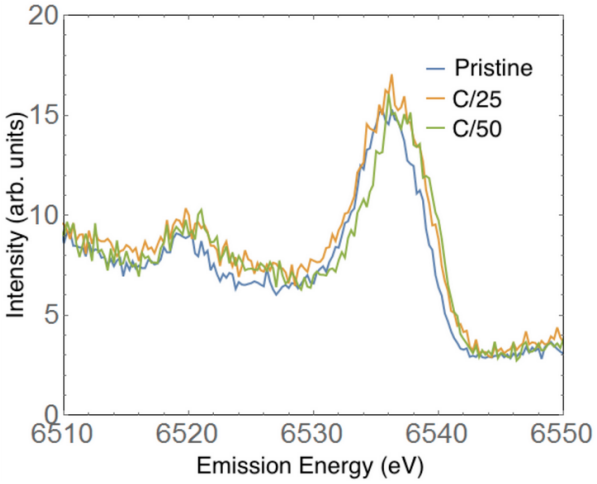

FIG. 8. Plot of the K-$\beta_{2,5}$ and K-β" features for $LiMn_2O_4$ at three different charge states. The K-$\beta_{2,5}$ is on the right and the K-β" on the left.

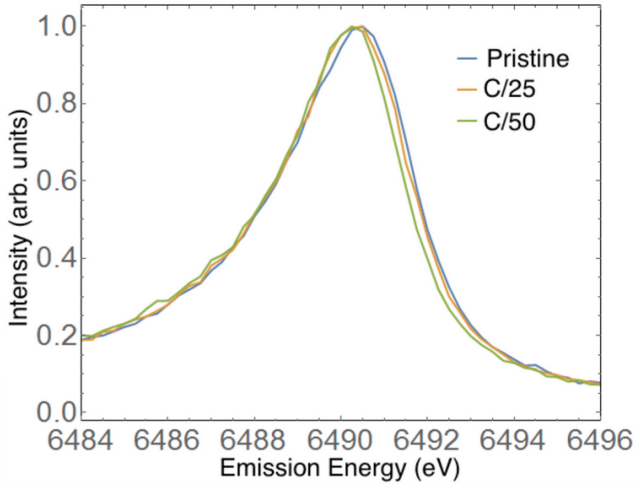

FIG. 7. Plot of the K-$\beta_{1,3}$ feature for $LiMn_2O_4$ at three different charge states.

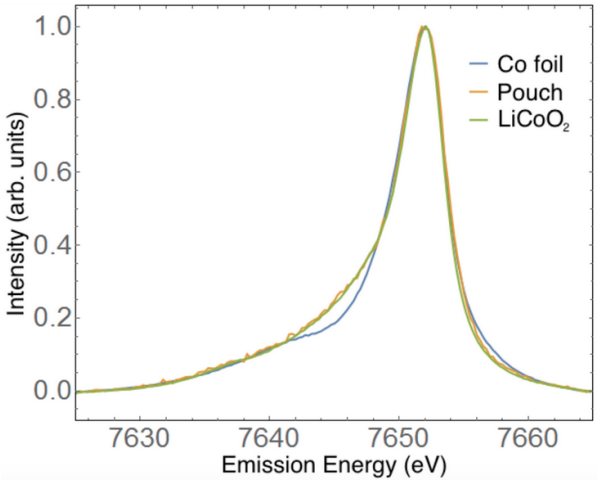

FIG. 9. Plot of the K-$\beta_{1,3}$ and K-β' features for the cobalt in the pouch cell battery.

B. Pouch Cell Battery

In situ spectra were taken of a pouch cell battery containing $Li_{1-x}Co_{1/3}Ni_{1/3}Mn_{1/3}O_2$ over the K-$\beta_{1,3}$ and valence regions. The crystal analyzer used was one appropriate for the cobalt in the pouch cell. These results were also compared to a cobalt foil and a lithium cobalt oxide in order to see whether the features observed were similar to expected features. The K-$\beta_{1,3}$ feature is shown in Fig. 8. The pouch cell shows good agreement with the $LiCoO_2$ with a very different K-β' feature from the cobalt foil. After averaging over 10 cycles, some of the valence features for the pouch cell were also resolved, as shown in Fig. 9. The feature to the right of the K-$\beta_{2,5}$ was not able to be resolved, but the rest of the valence showed good agreement with the $LiCoO_2$, as expected. The main limitations to these measurements are the low count rates. The pouch cell contains many layers, all of which absorb the x-rays as they enter and as they leave the battery. This decreases resolution capability. This made it especially difficult to measure the manganese in the pouch cell because bulk manganese had lower counts than bulk cobalt, possibly due to imperfections in the crystal analyzer. Diagnostics are being done now in order to improve these measurements in the future.

V. CONCLUSION

In situ XES spectra were obtained of $LiMn_2O_4$ and a pouch cell battery (containing $Li_{1-x}Co_{1/3}Ni_{1/3}Mn_{1/3}O_2$)

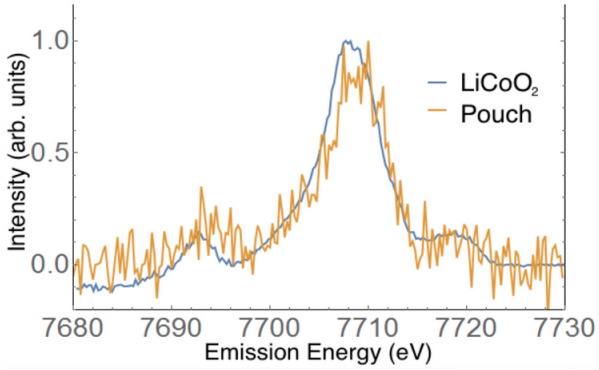

FIG. 10. Plot of the K-$\beta_{2,5}$ and K-β" features for the cobalt in the pouch cell battery as compared to a lithium cobalt oxide with no other transition metals. The K-$\beta_{2,5}$ is in the center and the K-β" on the left.

using a tabletop apparatus. The K-$\beta_{1,3}$/K-β' peaks and K-$\beta_{2,5}$/K-β" were resolved in the spectra. The peaks for the $LiMn_2O_4$ were consistent with the expected oxidation states given the charge of those samples.

Future studies for the $LiMn_2O_4$ material will make qualitative measurements of the oxidation state of the sample in different charge states using more reference samples. Future studies may also look more in-depth to the valence features in the spectra. There are now more ongoing studies of the nickel in the pouch cell battery. The absorbance of each layer of the pouch cell is also going to be measured in order to determine whether there can be improvements made to the battery that could help make XES measurements easier without sacrificing battery performance. Once these are done or once a better manganese crystal analyzer is obtained, the manganese in the pouch cell will also be measured.

This was the first *in situ* measurement of a pouch cell battery and showed that these measurements are possible, specifically using this tabletop system.

VI. ACKNOWLEDGEMENTS

I would like to thank Professor Jerry Seidler for being a wonderful mentor and providing support and guidance throughout the summer. I would also like to thank Evan Jarman, a graduate student with whom I worked closely, as well as the rest of the Seidler group for their help and encouragement. Ron Musgrave in the machine shop was also very helpful as I built various projects for my group. The INT REU program was run in an excellent manner by Deep Gupta, Alejandro Garcia, Shih-Chieh Hsu, Gray Rybka, Linda Vilett, and Farha Habib. I would also like to thank the NSF for funding this project, as well as Tim Fister's team at Argonne National Labs for providing the samples used.

[1] P. Glatzel and U. Bergmann, Coord. Chem. Rev. **249**(1-2), 65-95 (2005).
[2] G. T. Seidler, D. R. Mortensen, A. J. Remesnik, J. I. Pacold, N. A. Ball, N. Barry, M. Styczinski, and O. R. Hoidn, Review of Scientific Instruments **85**(11), 113906 (2014).
[3] J. B. Goodenough and K. Park, J. Am. Chem. Soc. **135**(4), 1167-1176 (2013).
[4] P. Shearing, Y. Wu, S. J. Harris, and N. Brandon, Electrochemical Society Interface **20**(3), 43 (2011).
[5] U. Bergmann and P. Glatzel, Photosynth. Res. **102**(2-3), 255-266 (2009).
[6] M. Giorgetti, ISRN Materials Science **2013** (2013).